Computer Modeling in Engineering & Sciences

Tech Science Press

DOI: 10.32604/cmes.2024.054059

ARTICLE

Concurrent Two–Scale Topology Optimization of Thermoelastic Structures Using a M–VCUT Level Set Based Model of Microstructures

Jin Zhou, Minjie Shao*, Ye Tian and Qi Xia*

State Key Laboratory of Intelligent Manufacturing Equipment and Technology, Huazhong University of Science and Technology, Wuhan, 430074, China

*Corresponding Authors: Minjie Shao. Email: minjieshao@mail.hust.edu.cn; Qi Xia. Email: qxia@mail.hust.edu.cn

Received: 17 May 2024 Accepted: 19 July 2024 Published: 27 September 2024

ABSTRACT

By analyzing the results of compliance minimization of thermoelastic structures, we observed that microstructures play an important role in this optimization problem. Then, we propose to use a multiple variable cutting (M–VCUT) level set-based model of microstructures to solve the concurrent two–scale topology optimization of thermoelastic structures. A microstructure is obtained by combining multiple virtual microstructures that are derived respectively from multiple microstructure prototypes, thus giving more diversity of microstructure and more flexibility in design optimization. The effective mechanical properties of microstructures are computed in an off-line phase by using the homogenization method, and then a mapping relationship between the design variables and the effective properties is established, which gives a data-driven model of microstructure. In the online phase, the data-driven model is used in the finite element analysis to improve the computational efficiency. The compliance minimization problem is considered, and the results of numerical examples prove that the proposed method is effective.

KEYWORDS

Two–scale structure; topology optimization; multiple variable cutting level set; data–driven; radial basis function; thermoelastic structure

1 Introduction

A thermoelastic structure in this study is subjected to both temperature changes and mechanical forces. Optimization of thermoelastic structures with the aim of compliance minimization leads to some unusual and interesting results, as discussed in our previous study [1], and this motivated the present work of concurrent two-scale topology optimization. When the classical Solid Isotropic Microstructure with Penalization (SIMP) method is applied to solve the thermoelastic problem, many "gray" densities persist in the optimized structures even when the penalty parameter is increased, as shown in Fig. 1. In fact, such a structure with "gray" densities is indeed better than a "black–white" structure for this optimization problem [1]. More importantly, recalling that the "gray" densities in the SIMP method represent isotropic microstructures, we see that introducing microstructures into the topology optimization of thermoelastic structures will have great significance.

According to the observation mentioned above, one can see that it would be better if the optimization of thermoelastic structures was solved in both the macro scale and the microscale so that

different microstructures can be properly distributed in the structure to match different requirements at different positions and directions.

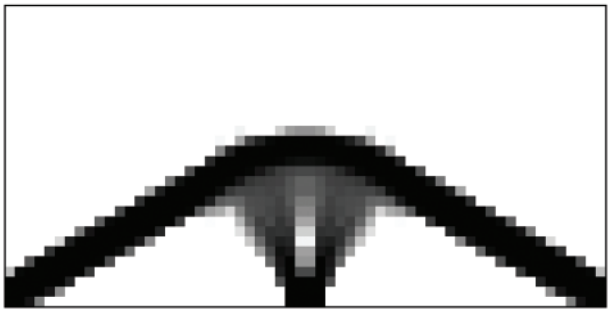

Figure 1: The optimized thermoelastic structure based on SIMP method, where gray densities imply isotropic microstructures

Two-scale topology optimization has caught much attention in the past decades, and many methods were proposed [2,3]. One important category of methods is based on the optimal microstructure prototype known a priori for the optimization problem or those specified by designer [4–7]. For example, in the minimum compliance problem under a single load, laminate microstructures have been rigorously shown to be optimal [8,9], and specified lattice structures are applied in two–scale optimization [10–13]. During the optimization, some parameters that describe the shape or topology of microstructures are iteratively updated, and different microstructures appear. In addition, based on this method, people also proposed to post-process the result to obtain a structure on a fine grid in the macro scale [14–18]. However, in this category of methods, the diversity of shape and topology of the optimized microstructure is not so rich.

The other category, often referred to as hierarchical or concurrent methods [19–23], does not require microstructural prototypes and allows microstructures at different locations of the structure to generate different configurations freely. This approach is more flexible, but the issue of connectivity between neighboring microstructures arises. Many efforts were made to address the connectivity issue [24–28].

Based on these previous research works, it is clear that the microstructure model has important impacts on two-scale topology optimization. Given this, an alternative microstructure model is proposed in the present study. The geometry of microstructure is described by the multiple variable cutting (M–VCUT) level set method proposed in our previous studies [29,30]. A microstructure is obtained by combining multiple virtual microstructures that are derived respectively from multiple microstructure prototypes. Then, the microstructures are treated as homogeneous materials in the macro scale, and their effective mechanical properties are dealt with respectively by two different approaches in an offline phase and an online phase. In the offline phase, the effective properties are computed by homogenization. Then, a mapping relationship between effective properties and design variables is established, which gives a data-driven model of microstructure. In the online phase, i.e., during the optimization, the data-driven model is used.

In our previous studies on the optimization of cellular structures [29,30], full-scale finite element analysis (FEA) with a fine mesh of elements was used, and this induces high computational costs. To improve the efficiency of the FEA, a data-driven model is employed. The benefits are two-fold. First, by deriving microstructures from multiple microstructure prototypes, the layouts of microstructures

become more diverse, thus providing more flexibility for design optimization, and at the same time the connectivity between microstructures is ensured. Second, because the computational costs of using such a data-driven model are much less than those of homogenization, the efficiency of FEA is improved.

2 Geometry Model and Homogenization of Microstructure

2.1 Geometry Model of Microstructure

A two–scale structure $\Omega \subset \mathbb{R}^d$ ($d = 2$ or 3) is optimized within a fixed reference domain $D \subset \mathbb{R}^d$, and the domain is decomposed into cells D^k ($k = 1...M$), i.e., $D = \cup_{k=1}^{M} D^k$. In each cell D^k, there may exist a microstructure Ω^k, i.e., $\Omega^k \subset D^k$. Similarly, a two–scale structure Ω is given by

$$\Omega = \cup_{k=1}^{M} \Omega^k \tag{1}$$

The microstructures Ω^k are described by using the M–VCUT level set method [29,30]. Each Ω^k is described by using multiple basic level set functions Φ_i^k ($i = 1...N$) and multiple cutting functions Ψ_i^k ($i = 1...N$). Each Φ_i^k represents a microstructure prototype and remains unchanged during the optimization. The cutting function is a horizontal plane with a constant height h_i^k here, i.e.,

$$\Psi_i^k(x) = h_i^k, \ \forall x \in D^k \tag{2}$$

The function Υ_i^k is used to represent the result of a cutting operation between Φ_i^k and Ψ_i^k, i.e.,

$$\Upsilon_i^k(x) = \Phi_i^k(x) - h_i^k, \ x \in D^k, \ k = 1 \ldots M, \ i = 1 \ldots N \tag{3}$$

After all the cutting operations are finished in D^k, N virtual microstructures $\widetilde{\Omega}_i^k$ defined by the function Υ_i^k are obtained as

$$\widetilde{\Omega}_i^k = \left\{ x \,|\, \Upsilon_i^k(x) < 0, \ x \in D^k \right\} \tag{4}$$

Examples of the cutting operation are shown in Fig. 2.

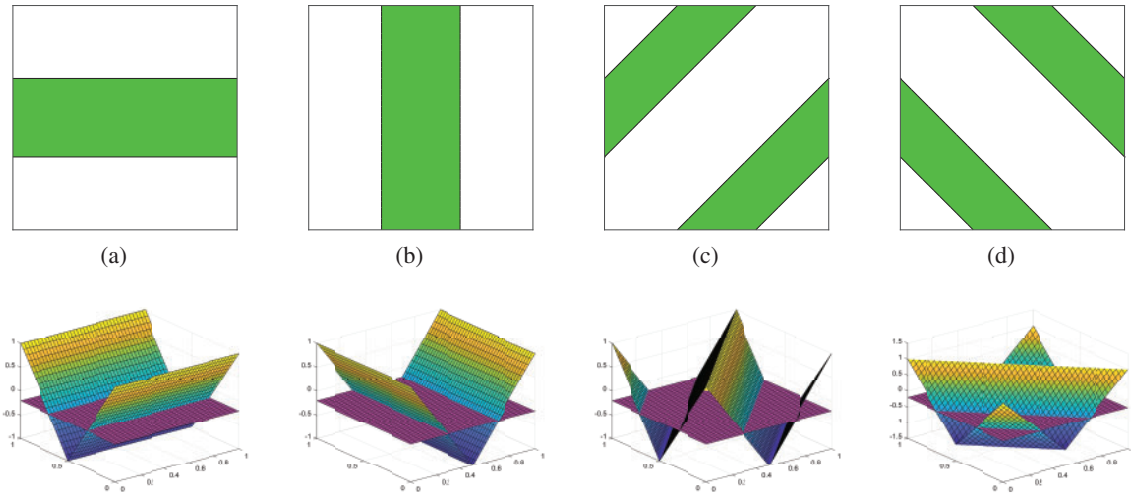

Figure 2: Description of the cutting operation. (a)–(d) four virtual microstructures obtained by the cutting operation, (e)–(h) four basic level set functions with the cutting planes shown in purple color

With all the virtual microstructures in D^k, one obtains an actual microstructures Ω^k by combining them together, i.e.,

$$\Omega^k = \cup_{i=1}^{N} \widetilde{\Omega}_i^k \tag{5}$$

The combination operation in Eq. (5) can be realized by

$$\Upsilon^k(x) = \min\left\{\Upsilon_1^k(x), \ldots, \Upsilon_N^k(x)\right\} \tag{6}$$

where Υ^k is the function used to define the actual microstructure Ω^k, i.e.,

$$\Omega^k = \left\{x \,|\, \Upsilon^k(x) < 0,\ x \in D^k\right\} \tag{7}$$

With the basic level setting function shown in Fig. 2, various actual microstructures can be obtained by changing the height of the cutting plane, as shown in Fig. 3.

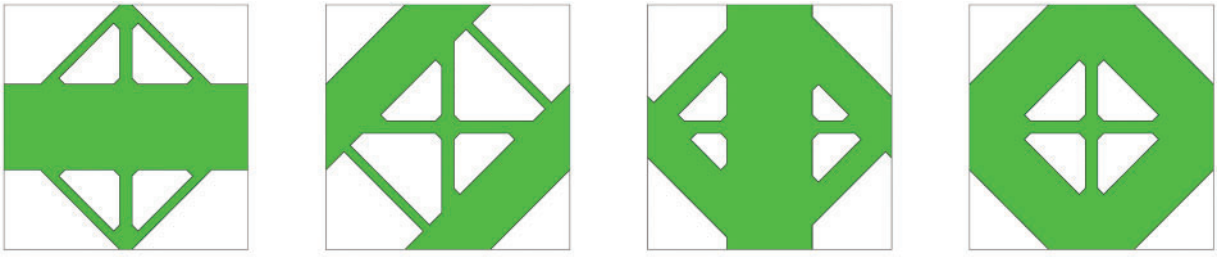

Figure 3: Actual microstructures generated based on the basic level set functions shown in Fig. 2. The heights of cutting planes for each microstructure are as follows: (a) $h_1 = -0.2$, $h_2 = -0.8$, $h_3 = -0.8$, $h_4 = -0.8$; (b) $h_1 = -0.8$, $h_2 = -0.8$, $h_3 = -0.2$, $h_4 = -0.8$; (c) $h_1 = -0.8$, $h_2 = -0.2$, $h_3 = -0.6$, $h_4 = -0.4$; (d) $h_1 = -0.8$, $h_2 - 0.8$, $h_3 = -0.2$, $h_4 = -0.2$

It should be noted that although the examples shown in Figs. 2 and 3 are obtained from the four microstructure prototypes, the number and type of prototypes are unrestricted in this method, and the prototypes can be modified according to different requirements.

In the optimization process, the only parameter of the cutting plane Ψ_i^k is the height h_i^k, which is the design variable, and all the heights h_i^k are changed according to the optimization algorithm, thus changing the virtual microstructure $\widetilde{\Omega}_i^k$, and then the actual microstructure Ω^k, and finally the double-scale structure Ω.

In the optimization, the design variables are the heights h_i^k of cutting planes. They are changed according to an optimization algorithm, thus changing the virtual microstructure $\widetilde{\Omega}_i^k$, then the actual microstructures Ω^k, and in the end the two-scale structure Ω.

2.2 Homogenization of Microstructure

In the two-scale optimization, the effective mechanical properties of microstructures are an important link between the macroscale and microscale. The homogenization method [4,31] is applied in an offline phase to compute the effective mechanical properties of the unit cells:

$$E_{ijkl}^H = \frac{1}{|Y|}\int_Y E_{pqrs}\left(\varepsilon_{pq}^{0(ij)} - \varepsilon_{pq}^{(ij)}\right)\left(\varepsilon_{rs}^{0(kl)} - \varepsilon_{rs}^{kl}\right) dY \tag{8}$$

where E_{pqrs} is the elastic tensor of the material of the microstructure; $|Y|$ is the volume of the cell; $\varepsilon_{pq}^{0(ij)}$ is the prescribed strain in macroscale; $\varepsilon_{pq}^{(ij)}$ denotes the strain in microscale defined as

$$\varepsilon_{pq}^{(ij)} = \varepsilon_{pq}\left(\chi^{ij}\right) = \frac{1}{2}\left(\chi_{p,\,q}^{ij} + \chi_{q,\,p}^{ij}\right) \tag{9}$$

where χ^{ij} is obtained by solving the equation

$$\int_Y E_{ijpq}\varepsilon_{ij}(v)\,\varepsilon_{pq}\left(\chi^{kl}\right)dY = \int_Y E_{ijpq}\varepsilon_{ij}(v)\,\varepsilon_{pq}^0\left(\chi^{kl}\right)dY,\ \forall v \in V \tag{10}$$

where v is the virtual displacement. For 2D problems, the results are rewritten in a matrix form as

$$\mathbf{D}^H = \begin{bmatrix} D_{11}^H & D_{12}^H & D_{13}^H \\ D_{21}^H & D_{22}^H & D_{23}^H \\ D_{31}^H & D_{32}^H & D_{33}^H \end{bmatrix}, D_{mn}^H = D_{nm}^H \tag{11}$$

3 Mapping Relationship between h_i and $\mathbf{D}^H$

Although numerical homogenization is a powerful tool for obtaining the effective elastic modulus of a microstructure, it leads to high computational costs for two–scale structures containing many microstructures. The costs are more prominent in the optimization that usually needs tens or hundreds of iterations. Therefore, in this paper, numerical homogenization is only done in an offline phase to generate data samples. Thereafter, these data samples are used to construct a simple numerical mapping model between the effective elastic modulus $\mathbf{D}^H$ and the design variables h_i. In the end, such a mapping model is used in the online optimization phase, more specifically in the macroscale FEA and sensitivity analysis. Because the computational costs of invoking such a mapping model are much less than those of homogenization, the efficiency of analysis and optimization of two-scale structures is improved. Such a mapping model can be regarded as a generalized model of anisotropic material microstructure whose role in structural optimization is similar to that of the power law model of the SIMP method.

3.1 Database of Microstructures

To establish the mapping relationship, we need a database that contains many data samples. The process of database creation is described below.

The range of all the basic level set functions Φ_i is $[-1,\ 1]$, as shown in Fig. 2. In addition, to ensure that empty microstructure and full microstructure can be obtained, the ranges of the cutting heights h_i are enlarged to $[-1.2,\ 1.2]$. Then, the cutting heights h_i are uniformly sampled in this interval with a spacing of 0.1. In other words, we have four microstructure prototypes, and we generate 25 virtual microstructures by changing the cutting height of each microstructure prototype with a spacing of 0.1. According to our numerical experience, such spacing is a proper compromise between the size of the database and the accuracy of the mapping relationship.

For each combination of the cutting heights h_i, we generate an actual microstructure and then create a data sample in the database. Therefore, if four microstructure prototypes are used, a total of 25^4 data samples are created in the database. Each data sample includes all the information required by the two-scale optimization, i.e., the cutting heights h_i, the elastic modulus D^H, and the volume V^H of the microstructure sample. Here, the V^H is obtained by numerical integration of the region occupied by the microstructure sample.

3.2 Radial Basis Function (RBF) Based Interpolation

With the database of microstructure, many methods can be used to construct the mapping relationship, for instance, the linear or low-order polynomials interpolation, neural networks, or surrogate models. In this paper, the RBF interpolation is used [32,33], because of its unique solvability, smoothness, and accuracy [34–38].

The Compact Support Radial Basis Function (CS–RBF) [32] is used to construct a local interpolation function by using a small amount of data around the evaluation point (denoted $\mathbf{h}$). Here, $\mathbf{h}$ is a column vector whose components are the cutting heights, i.e., $\mathbf{h} = [h_1, \ldots, h_N]^T$ and N is the number of cutting planes. The computational costs of such local interpolation are much lower than that of homogenization.

Using the CS–RBF interpolation, the elastic matrix D^H and the volume V^H of an actual microstructure with the cutting heights $\mathbf{h}$ can be obtained as

$$D^H_{mn}(\mathbf{h}) = \sum_{q=1}^{Q} \alpha_q^{mn} \phi\left(r_q(\mathbf{h})\right) \tag{12}$$

$$V^H(\mathbf{h}) = \sum_{q=1}^{Q} \beta_q \phi\left(r_q(\mathbf{h})\right) \tag{13}$$

where α_q^{mn} and β_q are the coefficients of the CS–RBFs; Q denotes the required number of data samples for local interpolation; r_q is a function of $\mathbf{h}$ defined as

$$r_q(\mathbf{h}) = \frac{1}{d_s}\sqrt{||\mathbf{h} - \hat{\mathbf{h}}_q||^2 + \sigma^2} \tag{14}$$

where $\hat{\mathbf{h}}_q = [\hat{h}_1, \ldots, \hat{h}_N]^T$ are the data points stored in the database; $||\mathbf{h} - \hat{\mathbf{h}}_q||$ is the Euclidean distance between $\mathbf{h}$ and $\hat{\mathbf{h}}_q$; d_s is the support radius, and it is set to 2; σ is a positive number set to 0.05. For better interpolation, the CS–RBF with C^2 continuity is chosen, as shown in Eq. (15).

$$\phi\left(r_q\right) = \max\left\{0,\ (1 - r_q)^4\right\}(4r_q + 1) \tag{15}$$

The coefficients α_q^{mn} and β_q of the CS–RBFs are obtained by solving equations that enforce values of interpolation functions that agree with data samples in the database. Such a system of linear equation of α_q^{mn} is given by

$$D^H_{mn}(\hat{\mathbf{h}}_q) = [\hat{D}^H_{mn}]_q, \quad q = 1, \ldots, Q \tag{16}$$

where $\hat{\mathbf{h}}_q$ is the cutting height vector of the q-th data sample in the local region of interpolation; $[\hat{D}^H_{mn}]_q$ is the effective elastic modulus related to $\hat{\mathbf{h}}_q$. Here, $\hat{\mathbf{h}}_q$ and $[\hat{D}^H_{mn}]_q$ are stored in the database. The matrix form of Eq. (16) is written as

$$\begin{bmatrix} \phi_{1,1} & \cdots & \phi_{1,Q} \\ \vdots & \ddots & \vdots \\ \phi_{Q,1} & \cdots & \phi_{Q,Q} \end{bmatrix} \begin{bmatrix} \alpha_1^{mn} \\ \vdots \\ \alpha_Q^{mn} \end{bmatrix} = \begin{bmatrix} [\hat{D}^H_{mn}]_1 \\ \vdots \\ [\hat{D}^H_{mn}]_Q \end{bmatrix} \tag{17}$$

where $\phi_{i,j}$ is given by

$$\phi_{i,\,j} = \phi\left(\frac{1}{d_s}\sqrt{||\hat{\mathbf{h}}_i - \hat{\mathbf{h}}_j||^2 + \sigma^2}\right), \quad i, j = 1 \ldots Q \tag{18}$$

Based on the four microstructures in Section 2.1, a mapping relationship between the design variables to the effective elasticity matrix of the microstructures is established. For example, when the design variable $\mathbf{h} = [-0.42,\ -0.87,\ -0.68,\ -0.35]^T$, the virtual microstructures are shown in Fig. 4a–d, and the actual microstructure is shown in Fig. 4e. The elastic matrix of the actual microstructure can be obtained by the RBF interpolation, and the result is

$$\mathbf{D}^H = \begin{bmatrix} 0.5254 & 0.1539 & -0.0265 \\ 0.1539 & 0.4404 & -0.0235 \\ -0.0265 & -0.0235 & 0.1615 \end{bmatrix} \tag{19}$$

Figure 4: Example of mapping relationship from design variables to microstructures: (a)–(d) four virtual microstructures, (e) actual microstructure

4 Optimization Problem of Two–Scale Thermoelastic Structures

The two–scale optimization of thermoelastic structures was investigated in many previous studies [39–41]. The optimization problems include multi-obiective problem [42], multi-material problem [43], and uncertainty problem [44]. In this paper, the compliance minimization of two-scale thermoelastic structures subjected to a uniform temperature change is considered.

$$\begin{aligned} \min \quad & C = \mathbf{f}_1^T\mathbf{u} + \mathbf{f}_2^T\mathbf{u} \\ \text{s.t.} \quad & \mathbf{K}\mathbf{u} = \mathbf{f}_1 + \mathbf{f}_2 \\ & h_{min} \le h_i^k \le h_{max} \\ & V - \overline{V} \le 0 \end{aligned} \tag{20}$$

where C is the compliance; $\mathbf{f}_1$ and $\mathbf{f}_2$ are the global thermal and global mechanical load vectors, respectively; $\mathbf{K}$ is the global stiffness matrix; $\mathbf{u}$ is the global displacement vector; h_{min} and h_{max} are respectively the upper and lower bounds of the design variable h_i^k; V is the volume of the two–scale structure, with $\overline{V}$ as the upper bound.

The global stiffness matrix $\mathbf{K}$ is written as

$$\mathbf{K} = \sum_{e=1}^{M} \int_{\Omega_e} \mathbf{B}^T \mathbf{D}_e^H \mathbf{B}\, \mathrm{d}x \tag{21}$$

where Ω_e is the e-th element; $\mathbf{D}_e^H$ denotes effective elastic modulus for the e-th element, and it is obtained by the CS–RBF interpolation; $\mathbf{B}$ is the strain-displacement matrix. In this study, each cell D^k is treated as a finite element in the macro-scale FEA.

The global thermal load vector $\mathbf{f}_1$ is given by

$$\mathbf{f}_1 = \sum_{e=1}^{M} \int_{\Omega_e} \mathbf{B}^T \mathbf{D}_e^H \boldsymbol{\varepsilon}^t \, \mathrm{d}x \tag{22}$$

where the thermal strain $\boldsymbol{\varepsilon}^t$ in plance stress state is given by

$$\boldsymbol{\varepsilon}^t = \alpha \Delta T \boldsymbol{\delta} \tag{23}$$

where α is the coefficient of thermal expansion of the material; ν is the Poisson's ratio; $\boldsymbol{\delta}$ is the unit tensor, which is $[1\ 1\ 0]^T$ in the planar problem; and ΔT denotes temperature change. The temperature change ΔT is assumed to be uniform. Note that α is independent of the microstructure composed of one material [45].

5 Sensitivity Analysis

To calculate the derivative of C concerning h_i^k, the objective function is rewritten by adding the state equation as a constraint

$$C = \mathbf{f}_1^T \mathbf{u} + \mathbf{f}_2^T \mathbf{u} - \widetilde{\mathbf{u}}^T (\mathbf{K}\mathbf{u} - \mathbf{f}_1 - \mathbf{f}_2) \tag{24}$$

where $\widetilde{\mathbf{u}}$ is the Lagrange multiplier, also known as the adjoint vector. Then, the derivative is

$$\frac{\partial C}{\partial h_i^k} = (\mathbf{u}^T + \widetilde{\mathbf{u}}^T) \frac{\partial \mathbf{f}_1}{\partial h_i^k} - \widetilde{\mathbf{u}}^T \frac{\partial \mathbf{K}}{\partial h_i^k} \mathbf{u} + (\mathbf{f}_1^T + \mathbf{f}_2^T - \widetilde{\mathbf{u}}^T \mathbf{K}) \frac{\partial \mathbf{u}}{\partial h_i^k} \tag{25}$$

Because $\mathbf{u}$ does not have an explicit relationship to the design variable h_i^k, calculation of $\dfrac{\partial \mathbf{u}}{\partial h_i^k}$ should be avoided. Therefore, the coefficient of this derivative is set to zero.

$$\mathbf{f}_1^T + \mathbf{f}_2^T - \widetilde{\mathbf{u}}^T \mathbf{K} = 0 \tag{26}$$

Comparing Eq. (26) with the state equation in the optimization problem Eq. (20), we get

$$\widetilde{\mathbf{u}} = \mathbf{u} \tag{27}$$

Applying the Eq. (27), we can simplify Eq. (25), so that the derivatives is

$$\frac{\partial C}{\partial h_i^k} = 2\mathbf{u}^T \frac{\partial \mathbf{f}_1}{\partial h_i^k} - \mathbf{u}^T \frac{\partial \mathbf{K}}{\partial h_i^k} \mathbf{u} \tag{28}$$

Then, substituting Eqs. (21) and (22) into (28), we get

$$\frac{\partial C}{\partial h_i^k} = 2\mathbf{u}_e^T \int_{\Omega_e} \mathbf{B}^T \frac{\partial \mathbf{D}_e^H}{\partial h_i^k} \boldsymbol{\varepsilon}^t \mathrm{d}x - \mathbf{u}_e^T \left(\int_{\Omega_e} \mathbf{B}^T \frac{\partial \mathbf{D}_e^H}{\partial h_i^k} \mathbf{B} \, \mathrm{d}x \right) \mathbf{u}_e \tag{29}$$

where $\mathbf{u}_e$ is the displacement vector.

The derivative of the elastic matrix $\mathbf{D}_e^H$ with respect to h_i^k in 2D problems is

$$\frac{\partial \mathbf{D}_e^H}{\partial h_i^k} = \begin{bmatrix} \frac{\partial [D_{11}^H]_e}{\partial h_i^k} & \frac{\partial [D_{12}^H]_e}{\partial h_i^k} & \frac{\partial [D_{13}^H]_e}{\partial h_i^k} \\ \frac{\partial [D_{21}^H]_e}{\partial h_i^k} & \frac{\partial [D_{22}^H]_e}{\partial h_i^k} & \frac{\partial [D_{23}^H]_e}{\partial h_i^k} \\ \frac{\partial [D_{31}^H]_e}{\partial h_i^k} & \frac{\partial [D_{32}^H]_e}{\partial h_i^k} & \frac{\partial [D_{33}^H]_e}{\partial h_i^k} \end{bmatrix} \tag{30}$$

According to the interpolation function in Eq. (12), we have

$$\frac{\partial [D_{mn}^H]_e}{\partial h_i^k} = \sum_{q=1}^{Q} \alpha_q^{mn} \frac{\partial \phi(r_q)}{\partial h_i^k} \tag{31}$$

According to the definition of CS–RBF in Eq. (15), we have

$$\frac{\partial \phi(r_q)}{\partial h_i^k} = \frac{\partial \phi}{\partial r_q} \frac{\partial r_q}{\partial h_i^k} = \max\left\{0,\ (1-r_q)^3\right\}(-20 r_q) \frac{\partial r_q}{\partial h_i^k} \tag{32}$$

Finally, according to Eq. (14), we have

$$\frac{\partial r_q}{\partial h_i^k} = \frac{h_i^k - \hat{h}_{q,\,i}}{d_s \sqrt{||\mathbf{h} - \hat{\mathbf{h}}_q||^2 + \sigma^2}} \tag{33}$$

The volume in the constraint function is the sum of the volumes of all the elements, which are also obtained from the mapping relationship. Therefore, the sensitivity analysis of the volume constraint function can also be performed by the above method. In this study, the Method of Moving Asymptotes (MMA) algorithm is used for optimization [46].

6 Numerical Example

Several examples of two–scale thermoelastic structural optimization are presented. Relevant properties of the material used in these examples are as follows: coefficient of thermal expansion $\alpha = 15.4 \times 10^{-3}(/\mathrm{K})$, Young's modulus $E = 1(\mathrm{Pa})$, and Poisson's ratio $\nu = 0.3$. To avoid singularities in FEA, an artificially weak material is defined with Young's modulus of $E = 10^{-3}(\mathrm{Pa})$ and other properties are the same.

Because the cutting heights in neighboring cells may not be continuous, the boundary of microstructures may exhibit a zigzag shape at the border of cells. Such a phenomenon can be relieved as the size of cells becomes smaller. In addition, we use a post-processing technique that smoothes the boundaries of structure [47]. In the post-processing, the cutting heights in adjacent cells are averaged at common nodes, and the node heights are used to obtain a new cutting surface by interpolation. This is similar to stress smoothing which takes the average of the element stresses as the node stress.

The convergence condition is given by

$$C_{err} = \frac{|\sum_{a=0}^{4} |C^{iter-a} - C^{iter-5-a}||}{\sum_{a=0}^{4} C^{iter-a}} \leq \delta_c \tag{34}$$

where C_{err} is the relative error of the objective function; *iter* is current number of iterations; δ_c is the bound of relative error. And, if *iter* reaches 500, the optimization will be stopped.

6.1 Example 1

The optimization problem and initial design are shown in Fig. 5. The structure is subjected to a uniform temperature change ΔT. The design domain is divided into 60×30 cells, and microstructures are defined by using the four prototypes shown in Fig. 2. In the macro-scale FEA, each cell is treated as a finite element. The upper bound of the structure volume is 20% of the design domain. Then, cutting height **h** of all cells are set to $[-0.5,\ -0.9,\ -0.6,\ -0.6]^T$ in the initial design Fig. 5b. The bounds of the design variables in the optimization equation Eq. (20) are set to $h_{min} = -1.2$ and $h_{max} = 1.2$. The "move" parameter is set to 0.01 when using the MMA method. The parameter δ_c in the convergence condition Eq. (34) is set to 0.05%.

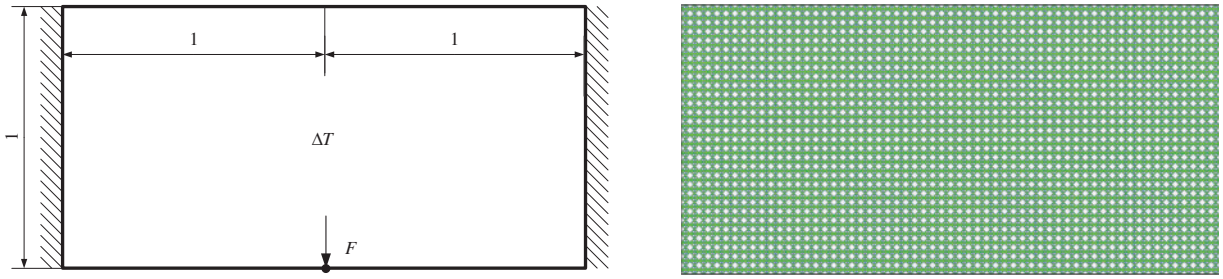

(a) (b)

Figure 5: The first example: (a) the design problem, (b) the initial design

The optimized structures with different temperature changes ΔT are shown in Fig. 6, and Table 1 shows their volume and compliance values. From the results, it is clear that the optimized structures change significantly with different temperature changes, which indicates that temperature cannot be ignored in structural design. Different types of microstructures, including porous cells, empty cells, and full-solid cells, are distributed in different regions of the structure.

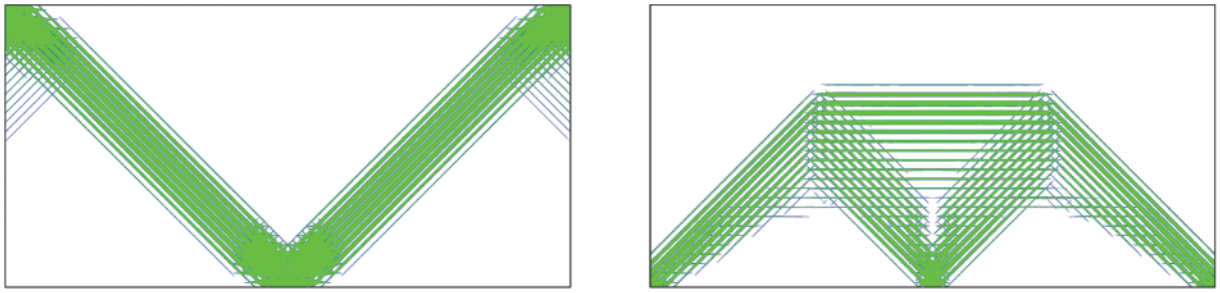

(a) (b)

Figure 6: (Continued)

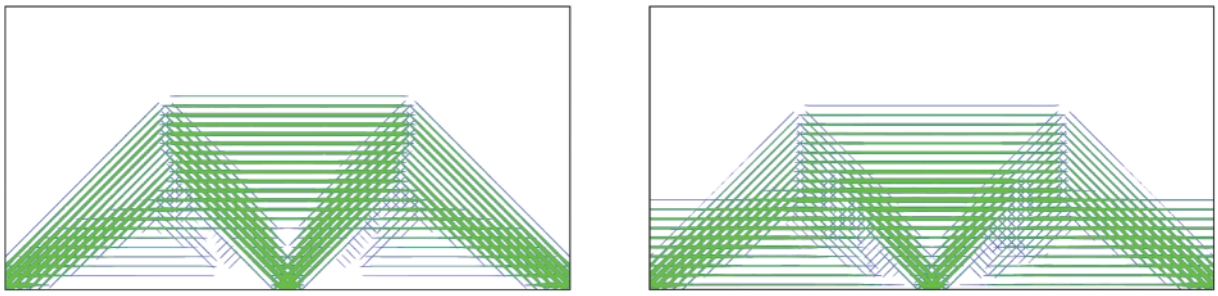

Figure 6: The optimized structure of the first example at different temperature changes: (a) $\Delta T = 0$, (b) $\Delta T = 10$, (c) $\Delta T = 15$, (d) $\Delta T = 20$

Table 1: Compliances and volumes of the optimized structures with different temperature changes

ΔT	0	10	15	20
Compliance	11.27	20.83	27.51	35.37
Volume	20.01%	20.00%	20.01%	20.00%

The design optimization problem is also solved only in the macroscale by using the SIMP method and the level set method. In the optimization, the temperature increment ΔT is set to 10 and the mesh used for FEA is 60×30. The optimized structures are shown in Fig. 7. The macroscale optimization results are compared with the previous one as shown in Table 2.

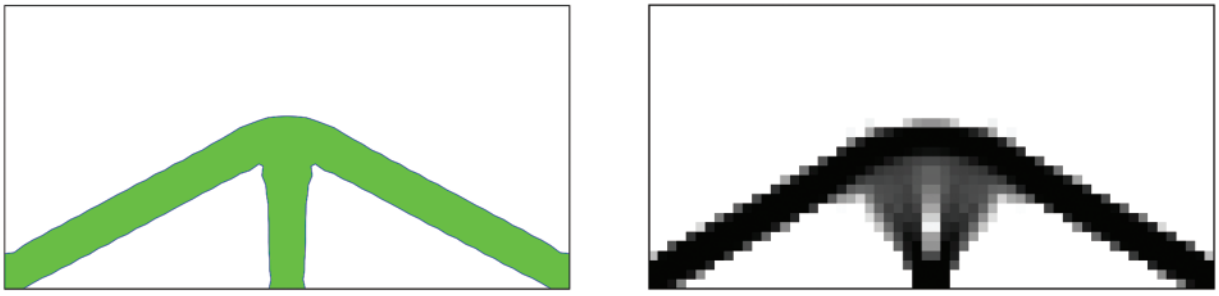

Figure 7: The optimized structures obtained through macroscale optimization methods with $\Delta T = 10$: (a) employing the level set method, (b) employing the SIMP method

Table 2: Comparison between two–scale and macroscale optimizations with $\Delta T = 10$

Method	Two–scale	Level set	SIMP
Compliance	20.83	29.08	28.40
Volume	20.09%	18.53%	20.00%

As can be seen from Table 2, the level set method results in the worst structural compliance. This is because the level set-based optimization has no microstructure, which is significant for thermoelastic structure optimization. In addition, one can see in Table 2 that the allowed volume of material is not fully used with the level set method. But the material volume fraction is always kept at 20% when using the optimization method proposed in this paper. This is because the proposed method provides multiple microstructures, and the use of microstructures provides a larger degree of freedom for structural design. This allows for a more rational material distribution, which will reduce the thermal loads, increase the structural stiffness, and reduce compliance.

In the SIMP method, the relative densities of the cells are the design variables, and a penalty parameter $p = 3$ is usually employed to drive the densities to either 1 or 0, i.e., a "black-white" design. However, as shown in Fig. 7b, the optimized structure has a large area of "gray" densities, but not a "black-white" design. Such a design is indeed the best solution given by the SIMP method, as discussed in our previous study [1]. Recall the name SIMP is "solid isotropic microstructure with penalization", one can see that these "gray" densities represent isotropic material microstructures. Therefore, we conclude that microstructures are helpful in this optimization problem. However, the isotropic microstructures are still not enough for the optimization to fully exploit its potential, and using various anisotropic microstructures in the optimization gives the best compliance among the three methods, as shown in Table 2.

Finally, to verify the advantage of using multiple microstructure prototypes, the optimization is also conducted by using only two microstructure prototypes, as shown in Fig. 8. The setting of optimization is kept the same as before. Fig. 9 shows the optimized structures, which have the compliance and volume shown in the Table 3. Comparing Table 3 with Table 1, one can see that using more microstructural prototypes yields better optimization results. In addition, the microstructures shown in Fig. 8 are orthotropic, and those shown in Fig. 2 are anisotropic. Because anisotropic microstructures offer more flexibility than orthotropic ones, the results of the optimization with the former are better than the latter.

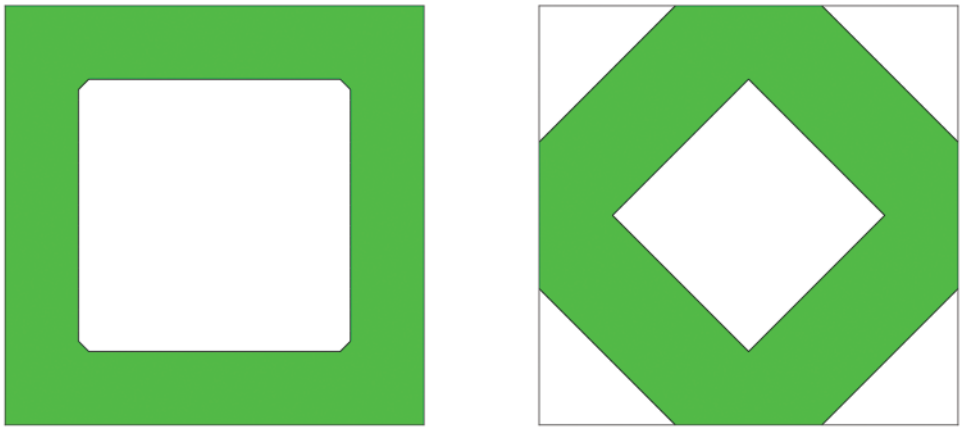

Figure 8: Two orthotropic microstructure prototypes

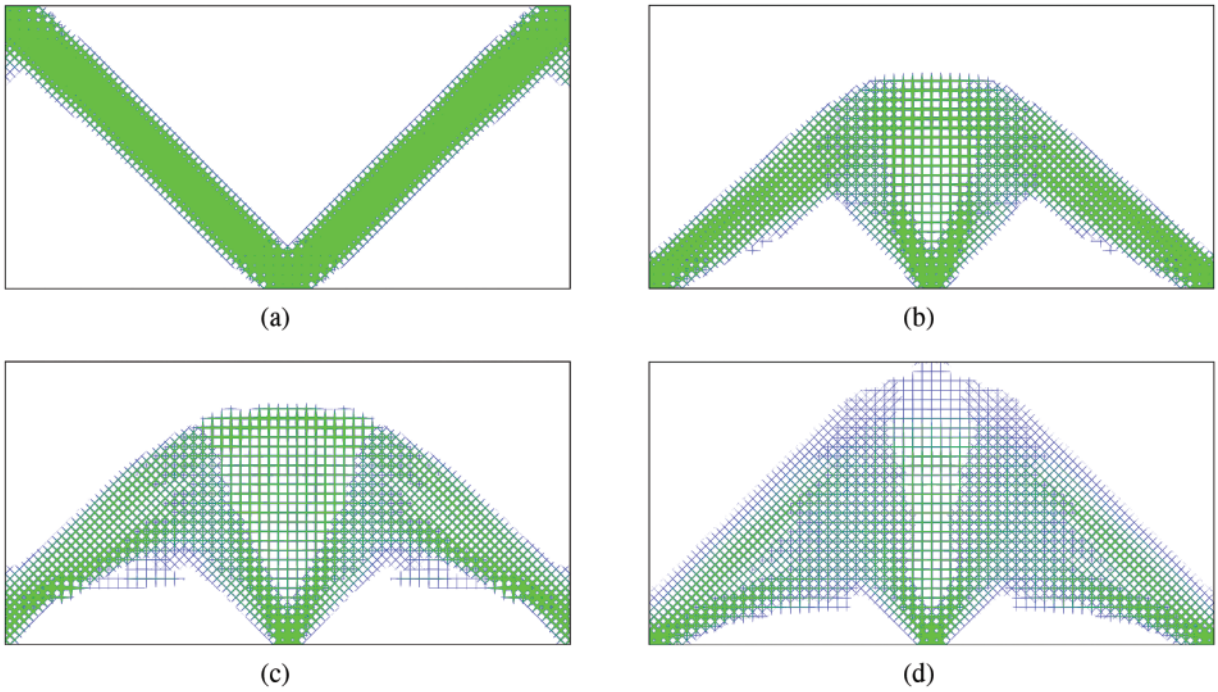

Figure 9: The optimized structures using two microstructure prototypes at different temperature changes: (a) $\Delta T = 0$, (b) $\Delta T = 10$, (c) $\Delta T = 15$, (d) $\Delta T = 20$

Table 3: Results of two–scale optimization using two microstructure prototypes

ΔT	0	10	15	20
Compliance	11.44	27.60	41.67	51.71
Volume	19.99%	20.00%	19.97%	17.51%

6.2 Example 2

This problem is the cantilever beam, as shown in Fig. 10. The structure is subjected to a uniform temperature change ΔT. The design domain is divided into 60×40 cells, and microstructures are defined by using the four prototypes shown in Fig. 2. In the macro-scale FEA, each cell is treated as a finite element. The upper bound of the structure volume is 50% of the design domain. The cutting heights $\mathbf{h}$ of all cells in the initial design are $[-0.5,\ -0.9,\ -0.6,\ -0.6]^T$. The bounds of the design variables are kept the same, i.e., $h_{max} = 1.2$ and $h_{min} = -1.2$. The "move" parameter is set to 0.005 when using the MMA method. The parameter δ_c in the convergence condition Eq. (34) is set to 0.05%.

The two-scale structure is optimized with different temperature increments ΔT. The optimized results can be seen in Fig. 11, and the volume and compliance values are shown in Table 4. It is clear that as the temperature increases, the number of full-solid cells gradually decreases and that of the porous cells increases. Therefore, one can see the significance of two-scale optimization for thermoelastic structures, which considers the microstructure in the optimization.

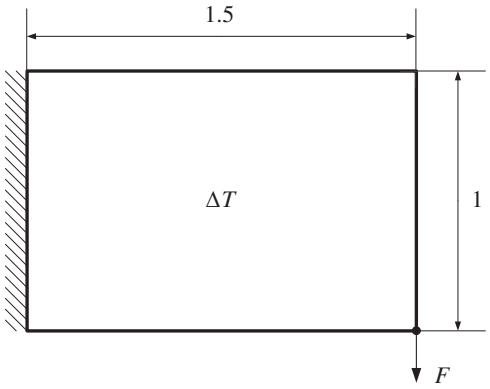

Figure 10: The design problem of the second example

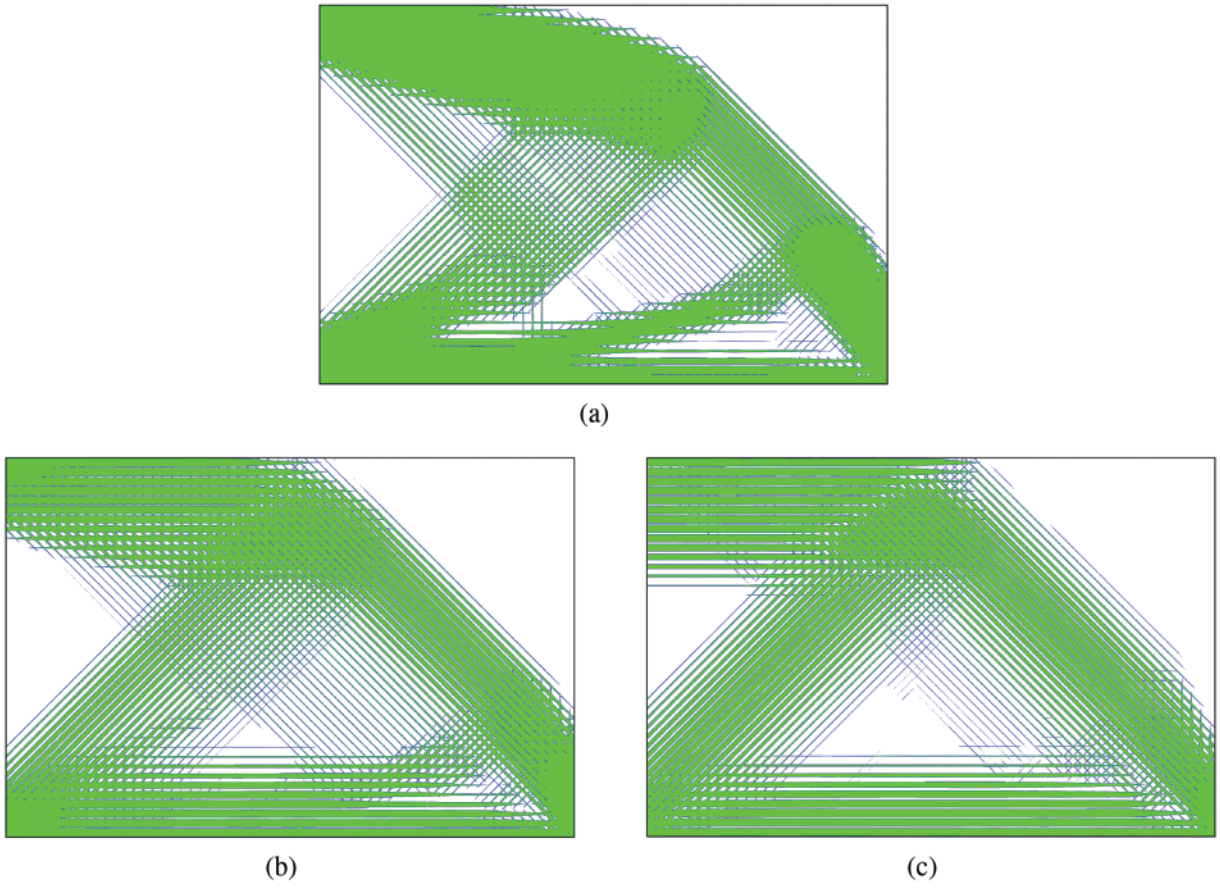

Figure 11: The optimized structure of the second example at different temperature changes: (a) $\Delta T = 0$, (b) $\Delta T = 5$, (c) $\Delta T = 10$

Table 4: Compliance and volume at different temperature changes

ΔT	0	5	10
Compliance	37.70	53.10	80.71
Volume	50.00%	49.99%	49.95%

6.3 Example 3

The previous numerical examples are all planar problems, but the approach presented in this paper can also be applied to three-dimensional (3D) problems, shown in Fig. 12. The boundary conditions for this problem are similar to those of Example 1: the two end faces of the structure are completely fixed, the middle of the bottom is subjected to a line load, and the structure is in a uniform temperature increment ΔT. The design domain is divided into $30 \times 15 \times 5$ cells, which are also used as finite elements in FEA. The upper bound of the structure volume is set to 20% of the design domain. Young's modulus of the material is set to $E = 200$(Pa) and the coefficient of thermal expansion $\alpha = 15.4 \times 10^{-5}$(/K).

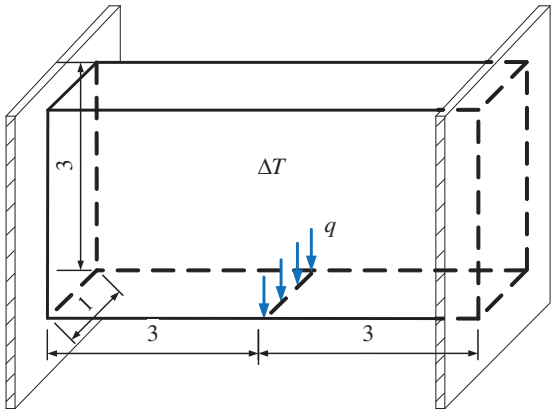

Figure 12: The 3D design problem of the third example

When the temperature increments ΔT are set to 5 and 10, the optimized structure is shown in Fig. 13. The microstructures of different regions in the structure are different, which is the result of the two-scale optimization. It is evident that in the upper face of Fig. 13a, the material in the middle of the structure was removed. As the temperature increases, more porous microstructures appear in Fig. 13b, which is the same tendency as in Fig. 9. The material distribution of the structure can also be clearly shown from the frontal views Fig. 13c,d, which are similar to the results of the planar examples. At the same time, the data-driven approach enhances the speed of structure optimization.

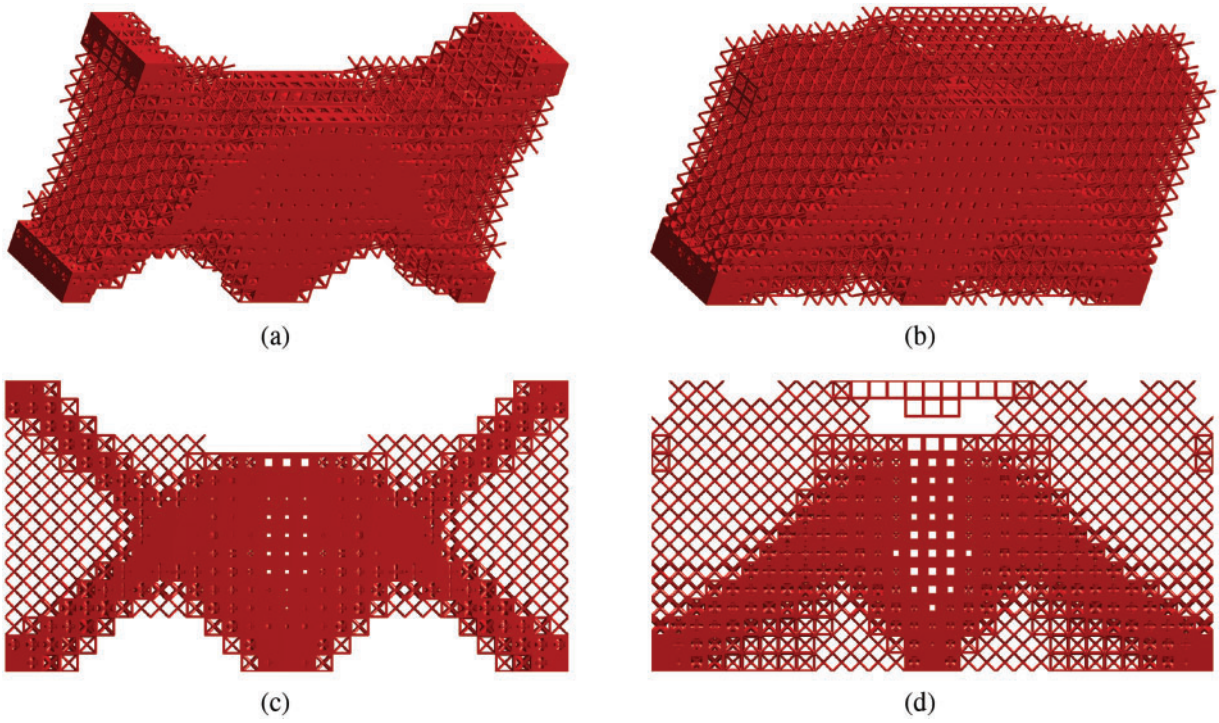

Figure 13: The optimized 3D structure at different temperature changes: (a) optimized result for $\Delta T = 5$ in the default view, (c) is the front view; (b) optimized result for $\Delta T = 10$ in the default view, (d) is the front view

7 Conclusion

In this paper, a data-driven model is integrated with the M–VCUT level set-based geometry model to solve the two–scale topology optimization of thermoelastic structures. The geometry of the microstructures is described using the M–VCUT level set method; the effective properties of the microstructure are calculated using the homogenization method in an offline phase; the RBF-based interpolation is employed to construct a data-driven model that describes the relationship between design variables and effective properties; this data-driven model is used in the FEA and sensitivity analysis. Because the costs of invoking such a data-driven model are much less than those of homogenization, the computational efficiency is improved.

From the numerical examples, one can see that the results of the proposed method are better than those of the macroscale optimization because various anisotropic microstructures are reasonably distributed into the macrostructure. In addition, one can also see that when more microstructure prototypes are used in the optimization, the results become better. Although four microstructure prototypes are used in the numerical examples in this study, the number and type of microstructure prototypes are unrestricted, and this flexibility is very important for obtaining better results in two-scale optimization.

Acknowledgement: The authors express their gratitude to Krister Svanberg for providing the MMA code support that allowed us to use it in this study.

Funding Statement: This research work is supported by the National Natural Science Foundation of China (Grant No. 12272144).

Author Contributions: The authors confirm contribution to the paper as follows: study conception and design: Jin Zhou, Qi Xia; data collection: Minjie Shao; analysis and interpretation of results: Jin Zhou, Minjie Shao, Ye Tian; draft manuscript preparation: Jin Zhou, Qi Xia. All authors reviewed the results and approved the final version of the manuscript.

Availability of Data and Materials: All data generated or analyzed during this study are included in this published article.

Ethics Approval: Not applicable.

Conflicts of Interest: The authors declare that they have no conflicts of interest to report regarding the present study.

References

1. Xia Q, Wang MY. Topology optimization of thermoelastic structures using level set method. Comput Mech. 2008;42:837–57.
2. Meng L, Zhang W, Quan D, Shi G, Tang L, Hou Y, et al. From topology optimization design to additive manufacturing: today's success and tomorrow's roadmap. Arch Comput Methods Eng. 2020;27:805–30.
3. Wu J, Sigmund O, Groen JP. Topology optimization of multi-scale structures: a review. Struct Multidiscipl Optim. 2021;63:1455–80.
4. Bendse MP, Kikuchi N. Generating optimal topologies in structural design using a homogenization method. Comput Methods Appl Mech Eng. 1988;71:197–224.
5. Chellappa S, Diaz AR, Bendse MP. Layout optimization of structures with finite-sized features using multiresolution analysis. Struct Multidiscip Optim. 2004;26:77–91.
6. Zhang P, Toman J, Yu Y, Biyikli E, Kirca M, Chmielus M, et al. Efficient design-optimization of variable-density hexagonal cellular structure by additive manufacturing: theory and validation. ASME J Mech Des. 2015;137:21004.
7. Wang YJ, Arabnejad S, Tanzer M, Pasini D. Hip implant optimization design with three-dimensional porous material of graded density. AMSE J Mech Des. 2018;140:111406.
8. Olhoff N, Ronholt E, Scheel J. Topology optimization of three-dimensional structures optimum microstructures. Struct Optim. 1998;16:1–18.
9. Rozvany GIN. Aims, scope, methods, history and unified terminology of computer-aided topology optimization in structural mechanics. Struct Multidiscip Optim. 2001;21:90–108.
10. Wang YJ, Xu H, Pasini D. Multiscale isogeometric topology optimization for lattice materials. Comput Methods Appl Mech Eng. 2017;316:568–85.
11. Wu ZJ, Xia L, Wang ST, Shi TL. Topology optimization of hierarchical lattice structures with substructuring. Comput Methods Appl Mech Eng. 2019;345:602–17. doi:10.1016/j.cma.2018.11.003.
12. Li D, Liao W, Dai N, Xie YM. Anisotropic design and optimization of conformal gradient lattice structures. Comput-Aided Des. 2020;119:102787. doi:10.1016/j.cad.2019.102787.
13. Wang J, Zhu J, Meng L, Sun QX, Liu T, Zhang WH. Topology optimization of gradient lattice structure filling with damping material under harmonic frequency band excitation. Eng Struct. 2024;309:118014. doi:10.1016/j.engstruct.2024.118014.
14. Pantz O, Trabelsi K. A post-treatment of the homogenization method for shape optimization. SIAM J Control Optim. 2008;47(3):1380–98. doi:10.1137/070688900.

15. Groen JP, Sigmund O. Homogenization-based topology optimization for high-resolution manufacturable microstructures. Int J Numer Methods Eng. 2018;113(8):1148–63. doi:10.1002/nme.5575.
16. Allaire G, Geoffroy-Donders P, Pantz O. Topology optimization of modulated and oriented periodic microstructures by the homogenization method. Comput Math Appl. 2019;78:2197–229. doi:10.1016/j.camwa.2018.08.007.
17. Zhu Y, Li S, Du Z, Liu C, Guo X, Zhang W. A novel asymptotic-analysis-based homogenisation approach towards fast design of infill graded microstructures. J Mech Phys Solids. 2019;124:612–33. doi:10.1016/j.jmps.2018.11.008.
18. Geoffroy-Donders P, Allaire G, Pantz O. 3-D topology optimization of modulated and oriented periodic microstructures by the homogenization method. J Comput Phys. 2020;401:108994. doi:10.1016/j.jcp.2019.108994.
19. Rodrigues HC, Guedes JM, Bendse MP. Hierarchical optimization of material and structure. Struct Multidiscip Optim. 2002;24:1–10. doi:10.1007/s00158-002-0209-z.
20. Coelho PG, Fernandes PR, Guedes JM, Rodrigues HC. A hierarchical model for concurrent material and topology optimisation of three-dimensional structures. Struct Multidiscip Optim. 2008;35:107–15. doi:10.1007/s00158-007-0141-3.
21. Xia L, Breitkopf P. Concurrent topology optimization design of material and structure within FE^2 nonlinear multiscale analysis framework. Comput Methods Appl Mech Eng. 2014;278:524–42.
22. Li H, Luo Z, Zhang N, Gao L, Brown T. Integrated design of cellular composites using a level-set topology optimization method. Comput Methods Appl Mech Eng. 2016;309:453–75.
23. Wang YG, Kang Z. Concurrent two-scale topological design of multiple unit cells and structure using combined velocity field level set and density model. Comput Methods Appl Mech Eng. 2019;347:340–64.
24. Zhou SW, Li Q. Design of graded two-phase microstructures for tailored elasticity gradients. J Mater Sci. 2008;43:5157–67.
25. Zhou SW, Li Q. Microstructural design of connective base cells for functionally graded materials. Mater Lett. 2008;62:4022–4.
26. Radman A, Huang X, Xie YM. Topology optimization of functionally graded cellular materials. J Mater Sci. 2013;48:1503–10. doi:10.1007/s10853-012-6905-1.
27. Cramer AD, Challis VJ, Roberts AP. Microstructure interpolation for macroscopic design. Struct Multidiscip Optim. 2016;53:489–500. doi:10.1007/s00158-015-1344-7.
28. Wang YQ, Chen FF, Wang MY. Concurrent design with connectable graded microstructures. Comput Methods Appl Mech Eng. 2017;317:84–101. doi:10.1016/j.cma.2016.12.007.
29. Liu H, Zong H, Shi T, Xia Q. M-VCUT level set method for optimizing cellular structures. Comput Methods Appl Mech Eng. 2020;367:113154. doi:10.1016/j.cma.2020.113154.
30. Xia Q, Zong H, Shi T, Liu H. Optimizing cellular structures through the M-VCUT level set method with microstructure mapping and high order cutting. Compos Struct. 2021;261:113298. doi:10.1016/j.compstruct.2020.113298.
31. Andreassen E, Andreasen CS. How to determine composite material properties using numerical homogenization. Comput Mater Sci. 2014;83:488–95. doi:10.1016/j.commatsci.2013.09.006.
32. Wendland H. Piecewise polynomial, positive definite and compactly supported radial functions of minimal degree. Adv Comput Math. 1995;4:389–96. doi:10.1007/BF02123482.
33. Buhmann MD. Radial basis functions: theory and implementations. In: Cambridge monographs on applied and computational mathematics. New York, NY: Cambridge University Press; 2004. vol. 12.
34. Wang SY, Wang MY. Radial basis functions and level set method for structural topology optimization. Int J Numer Meth Eng. 2006;65:2060–90. doi:10.1002/nme.1536.
35. Luo Z, Tong LMY, Wang SYW. Shape and topology optimization of compliant mechanisms using a parameterization level set method. J Comput Phys. 2007;227:680–705. doi:10.1016/j.jcp.2007.08.011.

36. Wei P, Li Z, Li X, Wang MY. An 88-line MATLAB code for the parameterized level set method based topology optimization using radial basis functions. Struct Multidiscip Optim. 2018;58:831–49. doi:10.1007/s00158-018-1904-8.
37. Jiu L, Zhang W, Meng L, Zhou Y, Chen L. A CAD-oriented structural topology optimization method. Comput Struct. 2020;239:106324. doi:10.1016/j.compstruc.2020.106324.
38. Tian Y, Shi T, Xia Q. Buckling optimization of curvilinear fiber-reinforced composite structures using a parametric level set method. Front Mech Eng. 2024;19(1):1–12. doi:10.1007/s11465-023-0780-0.
39. Yan J, Guo X, Cheng G. Multi-scale concurrent material and structural design under mechanical and thermal loads. Comput Mech. 2016;57:437–46. doi:10.1007/s00466-015-1255-x.
40. Xu B, Huang X, Zhou S, Xie YM. Concurrent topological design of composite thermoelastic macrostructure and microstructure with multi-phase material for maximum stiffness. Compos Struct. 2016;150:84–102. doi:10.1016/j.compstruct.2016.04.038.
41. Jiang H, Wei B, Zhou E, Wu Y, Li X. Robust topology optimization for thermoelastic hierarchical structures with hybrid uncertainty. J Thermal Stresses. 2021;44(12):1458–78. doi:10.1080/01495739.2021.1999877.
42. Deng J, Yan J, Cheng G. Multi-objective concurrent topology optimization of thermoelastic structures composed of homogeneous porous material. Struct Multidiscip Optim. 2013;47:583–97. doi:10.1007/s00158-012-0849-6.
43. Yan J, Sui Q, Fan Z, Duan Z. Multi-material and multiscale topology design optimization of thermoelastic lattice structures. Comp Model Eng Sci. 2022;130(2):967–86. doi:10.32604/cmes.2022.017708.
44. Zheng J, Ding S, Jiang C, Wang Z. Concurrent topology optimization for thermoelastic structures with random and interval hybrid uncertainties. Int J Numer Methods Eng. 2022;123(4):1078–97. doi:10.1002/nme.6889.
45. Sigmund O. Design of material structures using topology optimization (PhD Thesis). Technical University of Denmark: Denmark; 1994.
46. Svanberg K. The method of moving asymptotes-a new method for structural optimization. Int J Numer Methods Eng. 1987;24(2):359–73. doi:10.1002/nme.1620240207.
47. Liu H, Chen L, Bian H. Data-driven M-VCUT topology optimization method for heat conduction problem of cellular structure with multiple microstructure prototypes. Int J Heat Mass Transf. 2022;198:123421. doi:10.1016/j.ijheatmasstransfer.2022.123421.